

**Electron transport in waveguides
with spatially modulated strengths of the Rashba
and Dresselhaus terms of the spin-orbit interaction**

P. M. Krstajić, E. Rezasoltani, and P. Vasilopoulos

*Concordia University, Department of Physics,
7141 Sherbrooke Ouest Montréal, Québec H4B 1R6, Canada*

Abstract

We study electron transport through waveguides (WGs) in which the strengths of the Rashba (α) and Dresselhaus (β) terms of the spin-orbit interaction (SOI) vary in space. Subband mixing, due to lateral confinement, is taken into account only between the two first subbands. For sufficiently narrow WGs the transmission T exhibits a square-like shape as a function of α or β . Particular attention is paid to the case of equal SOI strengths, $\alpha = \beta$, for which spin-flip processes are expected to decrease. The transmission exhibits resonances as a function of the length of a SOI-free region separating two regions with SOI present, that are most pronounced for $\alpha = \beta$. The sign of α strongly affects the spin-up and spin-down transmissions. The results show that the main effect of subband mixing is to shift the transmission resonances and to decrease the transmission from one spin state to another. The effect of possible band offsets between regions that have different SOI strengths and effective masses is also discussed.

PACS numbers: 71.10.Pm, 72.25.-b, 73.21.-b

I. INTRODUCTION

There has been growing interest in the studies of spin-orbit interaction (SOI) in low-dimensional semiconductor structures made of III-V materials. The spin degree of freedom, often neglected in transport studies in semiconductors like silicon or germanium, may be important in other materials depending on the crystal structure, growth condition, and band alignment of the whole heterostructure. SOI, of relativistic origin, is a coupling between the intrinsic angular momentum (spin) and the orbital angular momentum in an external electric field. SOI manifests itself in semiconductor structures either due to the lack of (macroscopic) inversion symmetry of the whole structure, referred to as the Rashba SOI term [1], or due to the lack of inversion symmetry of the crystal structure, referred to as the Dresselhaus SOI term [2, 3]. The Rashba term can also be viewed as an effective magnetic field in the local frame, perpendicular to both momentum and electric field. Apart from the band alignment, it also depends on any external potential if it lifts the overall inversion symmetry which means it can be tuned by applying a bias [4–6]. On the other hand, the Dresselhaus SOI (DSOI) term arises as a consequence of the lack of inversion symmetry of the underlying crystal structure. It is commonly present in III-V semiconductors, like GaSb that has the zinc-blende structure, where the difference between cations and anions breaks the degeneracy of the band structure with respect to the spin degree of freedom, and is present in both bulk materials and semiconductor nanostructures. In low-dimensional semiconductor structures the DSOI manifests itself through terms that are linear and cubic in the wave vector k ; here we consider only the former, which is dominant for small k and is referred to as the [001] linear Dresselhaus term. There is an additional source of spin splitting present in semiconductor heterostructures due to the reduced symmetry at the interface [7, 8]. This manifestation of spin-orbit coupling is often named interface inversion symmetry or interface Dresselhaus SOI [9].

The studies of spin-dependent phenomena in semiconductor structures have been particularly intensified after the proposal of a spin-field effect transistor (FET) by Datta and Das [10]. This kind of the device would make use of the Rashba SOI only, by controlling the electron spin during its passage through the transistor. Ever since this proposal, there have been many refinements of the idea, notably the non-ballistic spin field-effect transistor [11] which would utilize both the Rashba and Dresselhaus terms of equal strength. In this design

it is expected that the transistor is robust against spin-independent scattering mechanisms. Further, a modification of the Datta-Das device has been proposed [12] whose function would be based on solely the DSOI. Motivated by this idea a wealth of related studies appeared in similar systems that dealt with spin-dependent transport, see, e.g, the review paper [13].

In previous work, coauthored by one of us, ballistic transport and spin-transistor behavior was studied, due only to the RSOI, in stubbed [14] WGs with constant strength α or unstubbed WGs with periodically modulated α [15]. An encouraging result was a nearly square-wave form of the transmission as a function of some stub parameters [14] or the strength [15] α . In this work we extend these studies by treating simultaneously both SOI terms, taking into account mixing between the lowest two subbands, and by studying *longitudinal* transmission resonances that occur when the length of a SOI-free region, separating two regions with SOI present, varies. As will be seen, if only one subband is occupied and both SOI terms are present, a phase difference $\phi = \tan^{-1}(-\beta/\alpha)$ arises in the spin eigenfunctions that strongly affects the spin-up and spin-down transmissions especially when ϕ changes sign. In Sec. II we present a model of a WG with two subbands, due to a lateral confinement, having nonzero mixing. We also derive the relevant dispersion relations and one-electron wave functions. In Sec. III we briefly explain the numerical procedure and present the main results. Concluding remarks follow in Sec. IV.

II. THEORETICAL MODEL

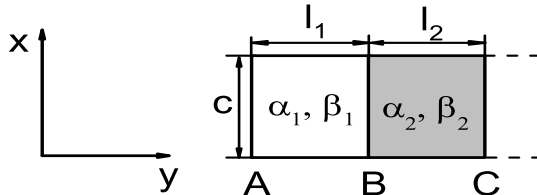


FIG. 1: Schematics of a WG unit, of width c , consisting of two segments with lengths l_1 , l_2 , and SOI strengths α_i , β_i , ($i = 1, 2$). The full unit is repeated along the y direction.

One unit of the WG we consider is shown in Fig. 1. It is made, e.g., of two layers of $\text{In}_x\text{Ga}_{1-x}\text{As}$ with different content of In, x_i , and has SOI strengths α_i and β_i . The WG consists of a finite number of such units periodically repeated in the y direction. Along the x direction a confining potential $V(x)$ is present that gives rise to bound states having

energies E_n . In principle a confinement along x could be created by etching after the usual 2D one along z . The two different growth directions which will be discussed are [010] and [110].

A. [010] grown waveguide

The one-electron Hamiltonian reads

$$H = H_0 + H_\alpha + H_\beta, \quad (1)$$

where H_0 is given by

$$H_0 = \frac{\hbar^2 \mathbf{k}^2}{2m^*} + V(x). \quad (2)$$

Here $\mathbf{k} = (k_x, k_y)$ is the wavevector of the electron and m^* its effective mass. H_α and H_β are the Rashba and Dresselhaus terms, respectively, given by

$$H_\alpha = \alpha[\sigma_x k_y - \sigma_y k_x], \quad H_\beta = \beta[\sigma_x k_x - \sigma_y k_y], \quad (3)$$

where $\sigma = (\sigma_x, \sigma_y, \sigma_z)$ are the Pauli spin matrices, and α, β the strengths of the Rashba and Dresselhaus terms, respectively. In writing Eq. (3) we assumed that the strength β depends mainly on the confinement along the z axis, only the linear-in-wave vector Dresselhaus term is important, and neglected any dependence on the lateral confinement along the x axis. The idea of linearly changing β by changing the well width along z has recently been reconfirmed in Ref. 16.

We write the total wave function as a linear combination of eigenstates of the unperturbed Hamiltonian

$$\Psi(x, y) = \sum_{n, \sigma} A_n^\sigma \phi_n(x) |\sigma\rangle e^{ik_y y}, \quad (4)$$

with n labelling the discrete subbands E_n due to the confining potential $V(x)$. The unperturbed states satisfy $H_0 |n, k_y, \sigma\rangle = E_n^0 |n, k_y, \sigma\rangle$, with $E_n^0 = E_n + \lambda k_y^2$ and $\lambda = \hbar^2/2m^*$. $\phi_n(x)$ is the solution of

$$\left[-\lambda \frac{d^2}{dx^2} + V(x) \right] \phi_n(x) = E_n \phi_n(x), \quad (5)$$

with the square-type $V(x)$ assumed high enough so that $\phi_n(x) = 0$ at the edges of the WG.

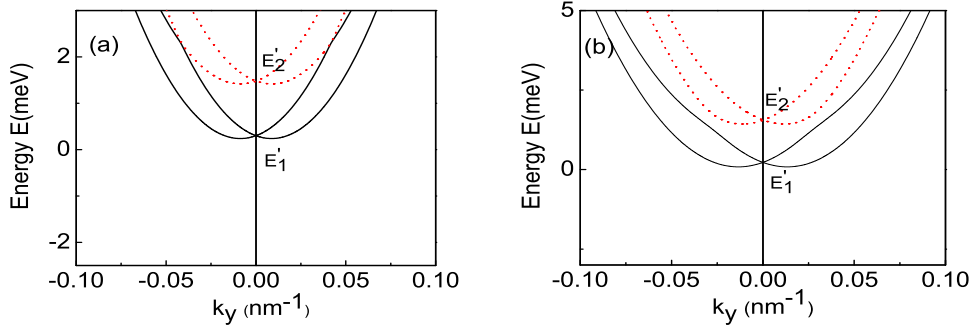


FIG. 2: Dispersion relation $E(k_y)$ for a WG, with equal SOI strengths $\alpha = \beta = \alpha_0 = 1 \times 10^{-11}$ eVm in (a) and for $\alpha = \alpha_0$, $\beta = 2\alpha_0$, in (b), where an anticrossing of the curves is visible. The interesections of the curves with the y axis, at $E'_{1,2}$, are close to the subband energies $E_{1,2}$ as explained in the text.

Using the full Hamiltonian given by Eqs. (1)-(3) and setting $\bar{E}_n = E_n^0 - E$ and $\gamma_{\pm} = \alpha \pm i\beta$, Eq. (4) leads to the secular equation

$$\begin{pmatrix} \bar{E}_n & \gamma_+ k_y \\ \gamma_- k_y & \bar{E}_n \end{pmatrix} \begin{pmatrix} A_n^+ \\ A_n^- \end{pmatrix} + \sum_m J_{nm} \begin{pmatrix} 0 & \gamma_- \\ -\gamma_+ & 0 \end{pmatrix} \begin{pmatrix} A_m^+ \\ A_m^- \end{pmatrix} = 0. \quad (6)$$

The factor J_{nm} embodies the subband mixing due to confinement and is nonzero for $n \neq m$,

$$J_{nm} = \int \phi_n(x) \phi'_m(x) dx. \quad (7)$$

To assess the magnitude of subband mixing we assume that the confining potential $V(x)$ is that of a quantum well with infinitely high walls at the edges of the WG whose width is c . Then $\phi_n(x) = (2/c)^{1/2} \sin(n\pi x/c)$ and considering mixing between the lowest two subbands the only non-vanishing matrix elements are $J_{12} = -J_{21} = \delta$, with $\delta = -8/(3c)$ [14]. Under these assumptions the eigenvalue problem resulting from Eq. (6) takes the form

$$\begin{pmatrix} E_1^0 & \gamma_+ k_y & 0 & \gamma_- \delta \\ \gamma_- k_y & E_1^0 & -\gamma_+ \delta & 0 \\ 0 & -\gamma_- \delta & E_2^0 & \gamma_+ k_y \\ \gamma_+ \delta & 0 & \gamma_- k_y & E_2^0 \end{pmatrix} \begin{pmatrix} A_1^+ \\ A_1^- \\ A_2^+ \\ A_2^- \end{pmatrix} = E \begin{pmatrix} A_1^+ \\ A_1^- \\ A_2^+ \\ A_2^- \end{pmatrix}, \quad (8)$$

where $E_1^0 = E_1 + \lambda k_y^2$, $E_2^0 = E_2 + \lambda k_y^2$. The eigenvalues, readily found from Eq. (19), are

$$\varepsilon_1^+ = [E_1^0 + E_2^0 - [G - F k_y]^2]^{1/2} / 2, \quad (9a)$$

$$\varepsilon_1^- = [E_1^0 + E_2^0 - [G + F k_y]^{1/2}] / 2, \quad (9b)$$

$$\varepsilon_2^+ = [E_1^0 + E_2^0 + [G + F k_y]^{1/2}] / 2, \quad (9c)$$

$$\varepsilon_2^- = [E_1^0 + E_2^0 + [G - F k_y]^{1/2}] / 2, \quad (9d)$$

with $F = 4[16\alpha^2\beta^2\delta^2 + \gamma^2\Delta E_{12}^2]^{1/2}$, $G = 4\gamma^2(\delta^2 + k_y^2) + \Delta E_{12}^2$ ($\gamma^2 = \alpha^2 + \beta^2$), and $\Delta E_{12} = E_2 - E_1$. The energy dispersions are given in the left panel of Fig. 2 for $\alpha = \beta = \alpha_0$ and in the right one for $\alpha = 0.5\beta = 2\alpha_0$.

Note that the energy dispersion curves do not start from E_1, E_2 at $\mathbf{k} = 0$ but rather from

$$E'_1 = [E_s - [4\gamma^2\delta^2 + \Delta E_{12}^2]^{1/2}] / 2, \quad (10a)$$

$$E'_2 = [E_s + [4\gamma^2\delta^2 + \Delta E_{12}^2]^{1/2}] / 2, \quad (10b)$$

where $E_s = E_1 + E_2$, as a result of the subband mixing.

Analytical expressions for the wavevector $k_y(E)$ as a function of the energy are complicated for the general case $\alpha \neq \beta$. Particular attention will be paid to the case $\alpha = \beta$ in which a suppression of spin-flip processes is expected [11, 17]. The relevant expressions are

$$k_{y1}^\pm = \left[\mp \alpha + [\alpha^2 - \lambda(E_s - D - 2E)]^{1/2} \right] / \sqrt{2}\lambda, \quad (11a)$$

$$k_{y2}^\pm = \left[\alpha \mp [\alpha^2 - \lambda(E_s + D - 2E)]^{1/2} \right] / \sqrt{2}\lambda, \quad (11b)$$

where $D = (8\alpha^2\delta^2 + \Delta E_{12}^2)^{1/2}$. From Eqs. (11a)-(11b) one can derive the critical energies

$$E_{cr1} = (E_s - D)/2 - \alpha^2/2\lambda, \quad (12)$$

$$E_{cr2} = (E_s + D)/2 - \alpha^2/2\lambda, \quad (13)$$

that determine the nature of the wave vectors k_{yi} in the following manner:

- $E \leq E_{cr1}$: for fixed i ($i = 1, 2$) all solutions k_{yi} are complex and conjugate in pairs;
- $E_{cr1} < E < E_{cr2}$: the solutions k_{y1} are real and the k_{y2} ones complex conjugate;
- $E \geq E_{cr2}$: all solutions k_{yi} are real.

For vanishing Dresselhaus strength $\beta \rightarrow 0$, the eigenvalue problem Eq. (19) simplifies significantly and the eigenvectors acquire [18] the simple analytical form

$$\Psi_1^+ = \frac{1}{C} \begin{pmatrix} 1 \\ 1 \\ r_B \\ -r_B \end{pmatrix}, \quad \Psi_1^- = \frac{1}{D} \begin{pmatrix} -1 \\ 1 \\ r_A \\ r_A \end{pmatrix}, \quad (14a)$$

$$\Psi_2^+ = \frac{1}{D} \begin{pmatrix} r_A \\ -r_A \\ 1 \\ 1 \end{pmatrix}, \quad \Psi_2^- = \frac{1}{C} \begin{pmatrix} r_B \\ r_B \\ -1 \\ 1 \end{pmatrix}, \quad (14b)$$

where $r_A = 2\alpha\delta/A$, $r_B = 2\alpha\delta/B$, $A = \delta E_{12} + 2\alpha k_y + \Delta E_+$, and $B = \delta E_{12} + 2\alpha k_y + \Delta E_-$. Further, $\Delta E_{\pm} = [(\Delta E_{12} \pm 2\alpha k_y)^2 + 4\alpha^2 \delta^2]^{1/2}$, $D = (2 + 2r_A^2)^{1/2}$, and $C = (2 + 2r_B^2)^{1/2}$.

If one goes further and neglects subband mixing, by taking the limit $\delta \rightarrow 0$, and if only the first subband is occupied, the original 4×4 eigenvalue problem, Eq. (19), reduces essentially to a 2×2 problem. Then the energy spectrum is given by

$$\varepsilon^{\pm} = E_1 + \lambda k_y^2 \pm (\alpha^2 + \beta^2)^{1/2} k_y \quad (15)$$

and the spinors acquire the simple form

$$\psi_e = \frac{1}{\sqrt{2}} \begin{pmatrix} 1 \\ \pm e^{i\phi} \end{pmatrix}, \quad \tan \phi = -\beta/\alpha. \quad (16)$$

This form of the spinors is important for the analysis of the transport problem through WGs. More precisely, one easily sees that the effect of the presence of the DSOI term is not just a simple increase of the overall SOI coupling, that is, $[\alpha^2 + \beta^2]^{1/2}$ in place of α ; one also has the change in the phase of the spinor component, that may significantly alter the transmission from one spin state to another. For illustrative purposes, we derive an analytical expression for the total transmission through a simple WG segment, with equal SOI strengths ($\alpha = \beta$) and length ℓ_2 , sandwiched between two SOI-free segments. The result is

$$T_x = \frac{1 + \cos^2 \epsilon}{2(1 + r \sin^2 \Delta_2 \ell_2)}, \quad (17)$$

where $\epsilon = \alpha \ell_2 / \sqrt{2} \lambda$, $r = (\Delta_1^2 - \Delta_2^2)^2 / 4 \Delta_1^2 \Delta_2^2$, $\Delta_1 = [4(E - E_1)\lambda]^{1/2} / 2\lambda$, and $\Delta_2 = [2\alpha^2 + 4(E - E_1)\lambda]^{1/2} / 2\lambda$. Once again, the effect of having both SOI terms present is not limited to the replacement $\alpha \rightarrow \sqrt{2}\alpha$; the transmission amplitude is also modulated through the factor ϵ in Eq. (17), if one compares with the simplest case ($\beta = 0, \alpha \neq 0$) [15]. From now on we will evaluate the transmission of spin states with z being the quantization axis.

B. Waveguide grown along the [110] direction

Apart from the usual growth direction along the crystallographic axis $\langle 001 \rangle$, the growth along the [110] direction is also important to investigate. The Dresselhaus term H_{β}

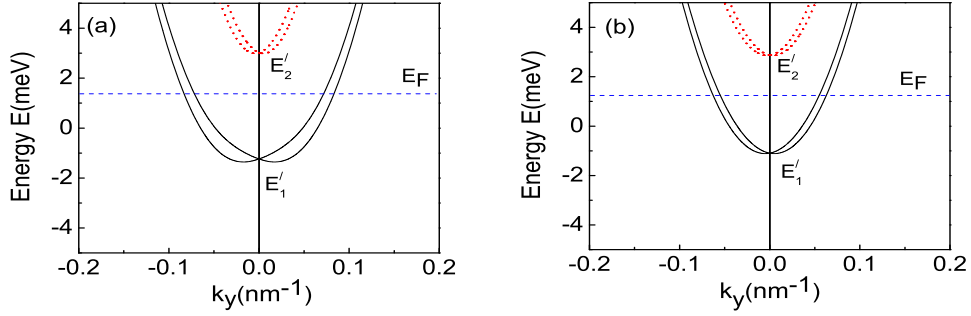


FIG. 3: Dispersion relation $E(k_y)$ for a WG grown along the [110] direction with equal SOI strengths in (a), $\alpha = \beta = \alpha_0 = 1 \times 10^{-11}$ eVm, and unequal ones in (b), $\alpha = \alpha_0$, $\beta = 2\alpha_0$.

has a somewhat simpler form [19]

$$H_\beta^{([110])} = -2\beta\sigma_z k_x, \quad (18)$$

while the Rashba term retains the same form since it is related to the structural (macroscopic) inversion asymmetry [20]. Employing a procedure similar to that in Sec. III A, we arrive at the eigenvalue problem

$$\begin{pmatrix} E_1^0 & \alpha k_y & 2i\beta\delta & \alpha\delta \\ \alpha k_y & E_1^0 & -\alpha\delta & -2i\beta\delta \\ -2i\beta\delta & -\alpha\delta & E_2^0 & \alpha k_y \\ \alpha\delta & 2i\beta\delta & \alpha k_y & E_2^0 \end{pmatrix} \begin{pmatrix} A_1^+ \\ A_1^- \\ A_2^+ \\ A_2^- \end{pmatrix} = E \begin{pmatrix} A_1^+ \\ A_1^- \\ A_2^+ \\ A_2^- \end{pmatrix}, \quad (19)$$

where the notation is the same as in Eq. (8).

The eigenvalues, readily found from Eq. (19), are given by Eq. (9) with F and G replaced, respectively, by $F_1 = 4\alpha\Delta E_{12}$ and $G_1 = 4\alpha^2(\delta^2 + k_y^2) + \Delta E_{12}^2 + 16\beta^2\delta^2$. The energy dispersions are given on the left panel of Fig. 3 for $\alpha = \beta = \alpha_0$ and on the right one for $\alpha = 0.5\beta = 2\alpha_0$. The dispersion curves are qualitatively different than those pertaining to the [010] direction due to the different form of the Dresselhaus term H_β . Further, the difference between equal and unequal SOI strengths is not as drastic as for WGs grown along the [010] direction.

III. NUMERICAL PROCEDURE AND RESULTS

As shown in Fig. 1, the WG consists of two segments, with different values of the Rashba and Dresselhaus couplings α and β , periodically repeated along the y axis. In each of the

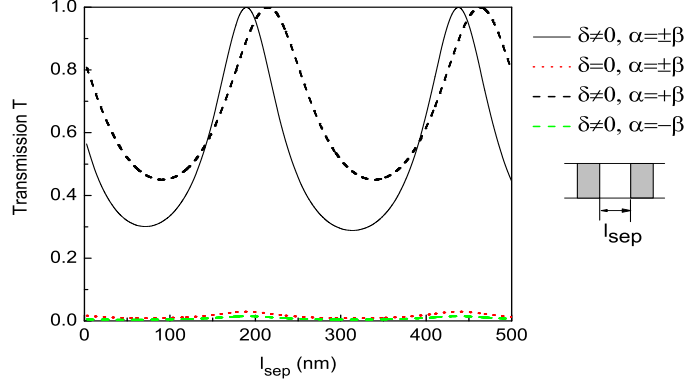


FIG. 4: Transmission through two segments, with $\alpha = \beta = 2\alpha_0$, versus the length ℓ_{sep} of the SOI-free region that separates them, for fixed $\ell_1 = \ell_2 = 95\text{nm}$. The solid curve corresponds to the total transmission while the dotted one to T^{+-} for $\alpha = \beta$ in both segments and the dash-dotted one to T^{+-} for $\alpha = -\beta < 0$ in the second segment. For comparison the total T is shown for zero subband mixing by the dashed curve. Here $\alpha_0 = 1 \times 10^{-11}\text{eVm}$.

segments the wave vector k_y is constant so that the wave function $\varphi_i(x, y)$ in the i -th segment is a superposition of plane wave-like states consisting of the eigenvectors d_j ($j = 1, \dots, 4$) of Eq. (19), in both directions along the y axis

$$\varphi_i(x, y) = \sum_j \left[c_i^{(j)} \cdot \psi_j e^{ik_{yj}y_s} + \bar{c}_i^{(j)} \cdot \bar{\psi}_j e^{-ik_{yj}y_s} \right] (2/c)^{1/2} \sin(n\pi x/c), \quad (20)$$

where $y_s = y - y_{0i}$. To find the complete solution, we first match the wave function at the interfaces between the i and $i + 1$ segments. Due to the presence of the off-diagonal elements in the Hamiltonian the continuity of the derivative of the wave function may not hold. A more general procedure is to require that the flux through materials with different SOI strengths or/and effective masses be conserved [21]. The velocity operator is given by

$$v_y = \frac{\partial H}{\partial p_y} = \frac{1}{\hbar} \begin{bmatrix} -2i\lambda\partial/\partial y & \gamma_+ & 0 & 0 \\ \gamma_- & -2i\lambda\partial/\partial y & 0 & 0 \\ 0 & 0 & -2i\lambda\partial/\partial y & \gamma_+ \\ 0 & 0 & \gamma_- & -2i\lambda\partial/\partial y \end{bmatrix}. \quad (21)$$

The continuity of the wave function at the interface $y = y_{i,i+1}$ gives $\varphi_{i+1}(x, y_{i,i+1}) = \varphi_i(x, y_{i,i+1})$ and that of the flux $\hat{v}_y \varphi_{i+1}(x, y)|_{y_{i,i+1}} = \hat{v}_y \varphi_i(x, y)|_{y_{i,i+1}}$. The unknown coefficients $c_i^{(j)}$ from Eq. (20) from one segment to another can be related through the transfer-matrix formalism by introducing the propagation matrix P_i and the boundary matching

matrix Q_i in each segment i . The transfer matrix [22] for the i -th segment is the matrix product

$$M(i, i + 1) = P_i^{-1} Q_i^{-1} Q_{i+1}. \quad (22)$$

In all numerical calculations we assumed that the incident electrons are (spin) unpolarized

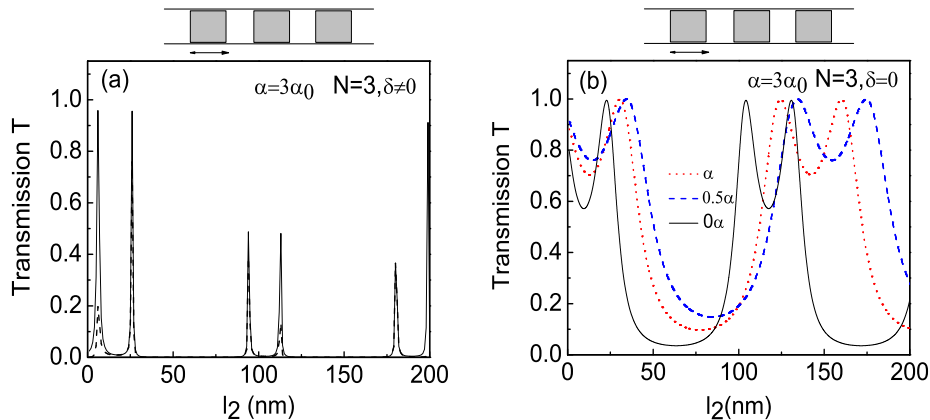


FIG. 5: (a) Transmission through three units versus length l_2 , for fixed $l_1 = 95\text{nm}$ and $\beta = \alpha = 3\alpha_0$. The solid curve is the total transmission and the dashed curve the T^{+-} one. (b) Same as in (a) but with zero subband mixing and three values of β : $\beta = \alpha = 3\alpha_0$ (dotted red curve), $\beta = 0.5\alpha$ (dashed blue curve), and $\beta = 0$ (solid black curve).

and we investigate only the transmission of one spin state, for instance, the spin-up one. We take the z axis as the quantization axis. We measure the SOI strengths in units of $\alpha_0 = 1 \times 10^{-11}$ eVm (Ref. [6]) and we first consider an energy $E = 0.13 \text{ meV} + E_1$ below the second subband.

First, we investigate the electron transmission through two segments having equal SOI strengths $\alpha = \beta$ and being separated by a SOI-free region of length l_{sep} . The results are shown in Fig. 4 for several cases: (1) α and β have the same sign in both segments; the total transmission is shown by the solid curve and the transmission from the spin-up to the spin-down state by the dotted curve; (2) the same as in case (1) but with negligible subband mixing ($\delta \rightarrow 0$, solid dashed curve); (3) $\alpha = -\beta$ in the second segment and T^{+-} shown by the dash-dotted curve. We note that the total transmission T is the same in cases (1) and (3), only the spin-up and spin-down transmissions are different in these cases. Here the value of α is taken to be $\alpha = 2\alpha_0$, close to the experimental value given in Ref. [4]. It can be inferred that changing the sign of α suppresses the transmission to the opposite spin

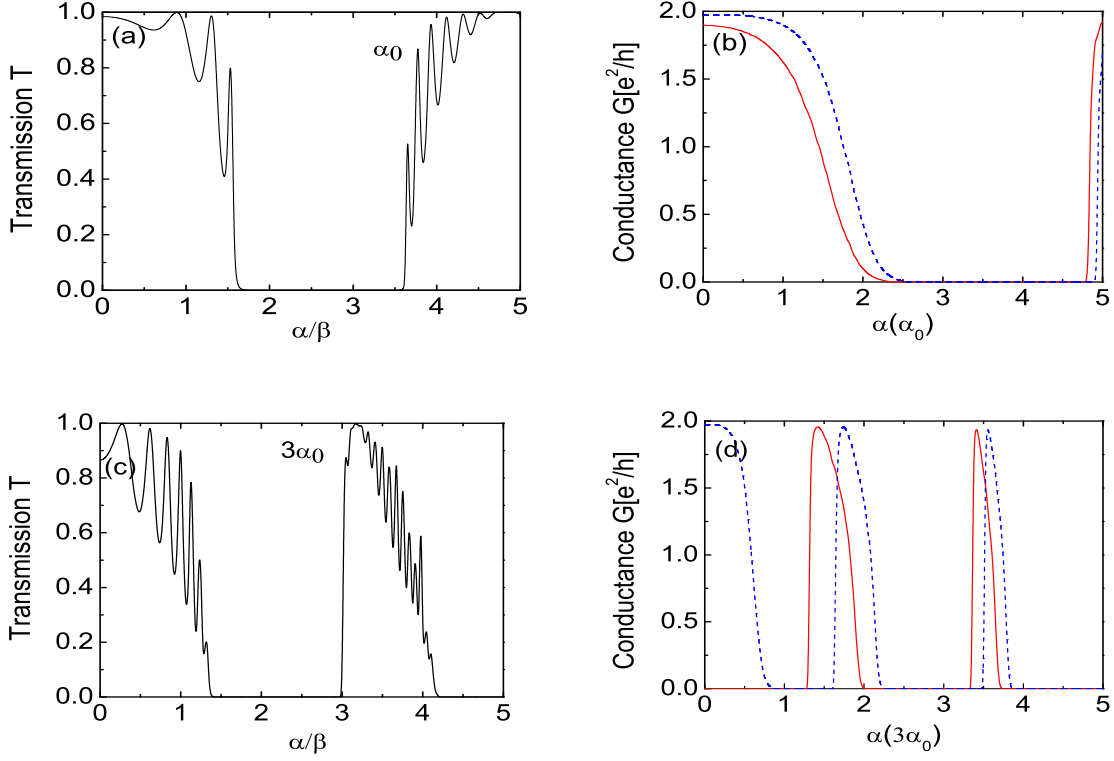


FIG. 6: (a), (c): Transmission through 20 units versus the ratio α/β with the SOI strengths given, respectively, in units of α_0 and $3\alpha_0$. (b), (d): Conductance G , at finite temperature $T = 0.2\text{K}$, versus α with β kept constant and equal, respectively, to α_0 and $3\alpha_0$ (solid red curves), and $\beta = 0$ (dashed blue curves). In all cases the unit lengths are $\ell_1 = \ell_2 = 95$ nm, the energy $E = 0.13$ meV, and the SOI is absent in the first segment of the unit.

state, while the subband mixing shifts the resonance maxima and has a minimal effect on the shape of the curve.

In Fig. 5 we plot the total transmission T through $N = 3$ units, as a function the length ℓ_2 , for fixed $\ell_1 = 95\text{nm}$ and $\alpha_1 = \beta_1 = 0$ in the SOI-free region, see Fig. 1, in two arrangements: with subband mixing present $\delta \neq 0$ in panel (a) and absent ($\delta = 0$) in panel (b). For illustrative purposes here we take $\alpha = 3\alpha_0$. Comparing the two graphs, one notices that the subband mixing introduces aperiodic features mainly in the T^{+-} transmission. Inspecting Fig. 5(b), one sees the effect of increasing β : the minima become deeper and shifted to the left.

It would be useful to investigate transport through a WG with significantly more than several units. The transmission through 20 units is shown in Fig. 6(a) and Fig. 6(c), as a

function of the ratio α/β . In panels (a) and (b) the SOI strengths are given in units of α_0 and those in panels (c) and (d) in units of $3\alpha_0$. For a clearer comparison the unit lengths $\ell_1 = \ell_2 = 95$ nm and the energy $E = 0.13$ meV are the same in all panels. Also, in all cases the SOI is absent in the first segment of the unit. Only ballistic transport was considered and the aim of taking a large number of units, N , is to demonstrate the near binary behaviour of the transmission [23]. This is readily seen by contrasting the upper with the lower panels. Notice though that the lower panels involve rather big SOI strengths.

Apart from the transmission T , the conductance G provides valuable information about the nanostructure especially at finite temperatures. G is given by the standard expression

$$G = \frac{e^2}{h} \int T(E)(-df/dE)dE, \quad (23)$$

where f is the Fermi-Dirac distribution. In Fig. (6)(b)

we show G for the same WG, at finite temperature $T_0 = 0.2$ K, as a function of α with β kept constant and equal, respectively, to α_0 and $3\alpha_0$ (solid red curves), and $\beta = 0$ (dashed blue curves). As can be seen, the dashed and dotted curves coincide since the SOI strength is the same in units of α_0 . The conductance when $\alpha = 0$ or $\beta = 0$ starts from 2 since then the WG is completely transparent (no SOI), whereas when both SOI terms are present G starts from a value between 1 and 2 due to phase $\phi \neq 0$ and a non-trivial energy dispersion $E(k_y)$, see Eqs. 15 and (16). In all cases the first segment of the unit has zero SOI. For higher

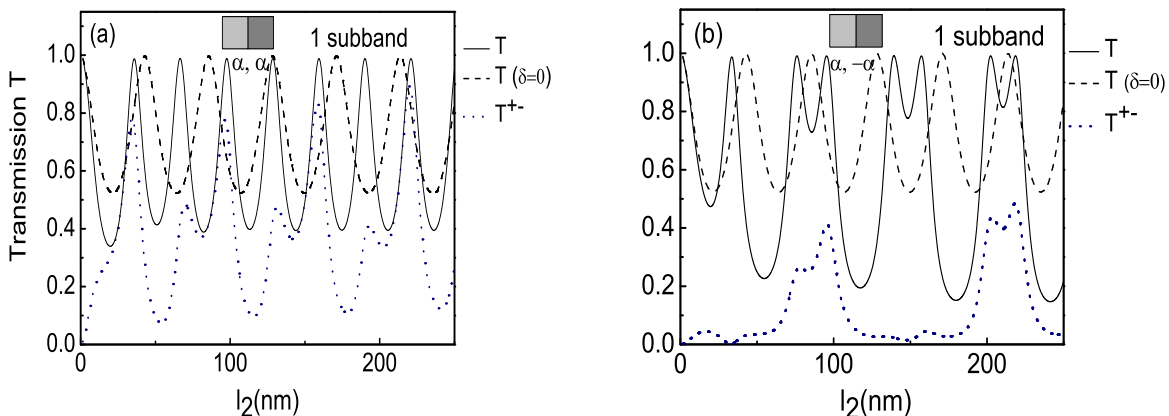


FIG. 7: (a) Transmission through two *successive* WG segments, of length ℓ_2 and strengths $\alpha = \beta = 2\alpha_0$, versus ℓ_2 . The solid curve is the total transmission and the dotted curve the T^{+-} one. The dashed curve shows the total transmission for zero mixing. (b) As in (a) but with $\alpha = -2\alpha_0$ in the second segment. The energy is $E = E_1 + 0.2$ meV.

values of the SOI strengths, $\beta = 3\alpha_0$ (dashed curve in Fig. 6(d)) the conductance exhibits a more binary behavior. For higher temperatures the qualitative behavior of G remains the same but the dips get shallower. We now assess the dependence of the transmission T on the phase ϕ . In Fig. 7 we show T through two successive WG segments, with the same length ℓ_2 and strength $\beta = 2\alpha_0$, versus ℓ_2 . Panel (a) is for $\alpha = 2\alpha_0$ and panel (b) for $\alpha = -2\alpha_0$. The solid curves show the total transmission while the dotted ones correspond to T^{+-} . For comparison, the values of the total transmission for zero mixing ($\delta = 0$) are shown as dashed curves. Comparing the two graphs one sees a strong effect the change of the sign of α has on the spin-down contribution which is almost filtered out for $\alpha = -2\alpha_0$ and ℓ_2 smaller than about 60 nm as well as for ℓ_2 approximately in the range 110 nm–180 nm .

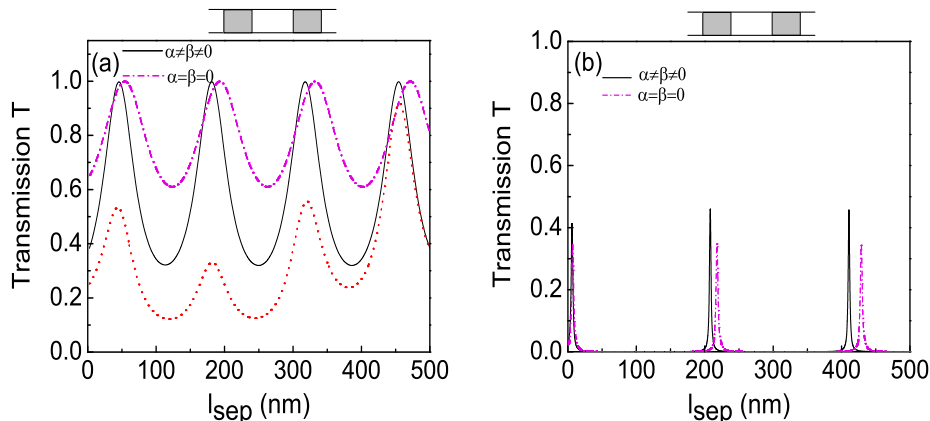


FIG. 8: Transmission through two $\text{In}_{x_2}\text{Ga}_{1-x_2}\text{As}$ segments, with $\alpha_2 = \beta_2 = \alpha_0$ and $x_2 = 0.2$, versus the length ℓ_{sep} of a $\text{In}_{x_1}\text{Ga}_{1-x_1}\text{As}$ segment that separates them with $\alpha = 0$, lengths $\ell_1 = \ell_2 = 95$ nm, $x_1 < x_2$, and $\beta_1 = \alpha_0/2$. Panel (a) is for pure GaAs ($x_1 = 0$) and a band offset $\Delta V = 0.23\text{eV}$ and panel (b) for $x_1 = 0.1$ and an offset $\Delta V \approx 0.12\text{eV}$. The solid (dash-dotted) curves show the total transmission when the SOI is present (absent, $\alpha_i = \beta_i = 0$). In addition, the red dotted curve in panel (a) shows the T^{+-} transmission.

At this point one may wonder how realistic the difference in SOI strengths is from one region to another or how it can be changed. Firstly, one can use the same material throughout the WG and instead apply gates that can change α , from region 1 to region 2, by a factor of 2 to 5. Secondly, if one uses different materials for regions 1 and 2, a band offset exists between them, i.e., $V(y)$ is not everywhere zero. As is well known, the Rashba term is controlled by an external gate and is taken to be zero within the layer made of

$\text{In}_{x_1}\text{Ga}_{1-x_1}\text{As}$. That is, one can take $\alpha_1 \approx 0$ but keep $\beta_1 \approx \alpha_0/2$ in the first segment, since it was assumed that $x_1 < x_2$. As usual we take $|\alpha_2| = |\beta_2| = \alpha_0$ for $\text{In}_{x_2}\text{Ga}_{1-x_2}\text{As}$. In Fig. 8(a) we show the case when the two $\text{In}_{x_2}\text{Ga}_{1-x_2}\text{As}$ segments are separated by a pure GaAs segment ($x_1 = 0$), free of the Rashba SOI, as a function of the separation length ℓ_{sep} . For an indium content $x = 0.2$, the conduction band mismatch between pure GaAs and $\text{In}_x\text{Ga}_{1-x}\text{As}$ is experimentally determined [24] to be 0.23eV. In

Fig. 8(b) we show the transmission through two $\text{In}_{x_2}\text{Ga}_{1-x_2}\text{As}$ ($x_2 = 0.2$) segments separated by a RSOI-free segment but now made of $\text{In}_{x_1}\text{Ga}_{1-x_1}\text{As}$ with $x_1 = 0.1$.

In the case we consider, $x_1 < x_2$, we assume $\Delta V \approx 0.12\text{eV}$, for $x_2 = 0.2$. The effective masses of $\text{In}_{0.2}\text{Ga}_{0.8}\text{As}$ and $\text{In}_{0.1}\text{Ga}_{0.9}\text{As}$ are 0.06 and 0.064, respectively [25]. We have taken into account this effective-mass difference between the two materials through the matching of the flux at the interfaces. The solid and dashed-dotted curves show the total transmission with and without SOI present, respectively. As shown, with a band offset present the transmission is smaller. The higher content of indium results in narrower transmission peaks when plotted vs ℓ_{sep} . In both cases, the peak-to-valley ratio is enhanced by the presence of SOI, thus improving the performance of a WG as a possible transistor. We further notice that, although the band offset is large compared to the change in the conduction-band structure caused by the SOI, in the order of a few meV, the influence of the SOI, through the phase factor in Eq. (16), is still important and changes the period of the transmission.

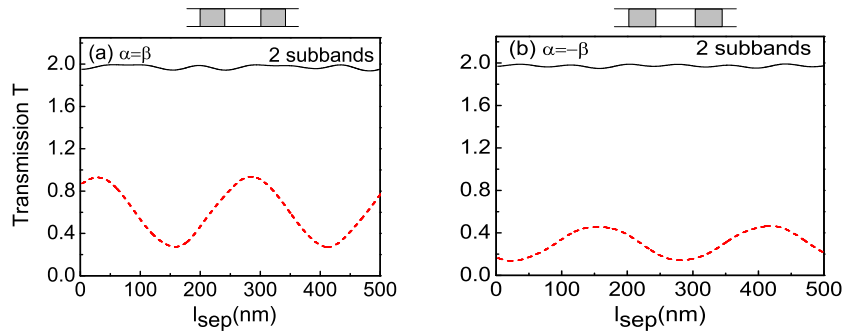


FIG. 9: (a) Transmission through two *simple* units versus their separation ℓ_{sep} for fixed $\ell_1 = \ell_2 = 100$ nm and $\alpha = \beta = \alpha_0$, when *both subbands* are occupied. The solid curve shows the total transmission and the dashed one the component T^{+-} . (b) Same as in (a) but with the second unit having a negative α , i.e., $\alpha = -\alpha_0$. The energy is $E = E_1 + 1.6$ meV.

Next, we consider the situation when both subbands are occupied, which occurs for $E > E'_2$. The electron transmission was evaluated through two simple units ($|\alpha| = \beta = \alpha_0$)

separated by a SOI-free region of length ℓ_{sep} . The total transmission T (solid curve) and the transmission from the spin-up to the spin-down state T^{+-} (dashed curve) of the second subband are shown in Fig. 9(a), when both units have positive strength α , and in Fig. 9(b) when the second unit has a negative α . In both cases the total transmission is close to unity, as a result of the high value of the Fermi energy, $E_F = 1.6$ meV, while the value of T^{+-} is suppressed when the Rashba coupling changes sign as in the case of only one subband occupied, see Fig. 4. One can see the filtering effect only in particular components of the transmission, while the total transmission varies very little with ℓ_{sep} . We emphasize that the shape and values of T^{+-} are more sensitive to changes in the energy and the strength α than in the case when only one subband is occupied.

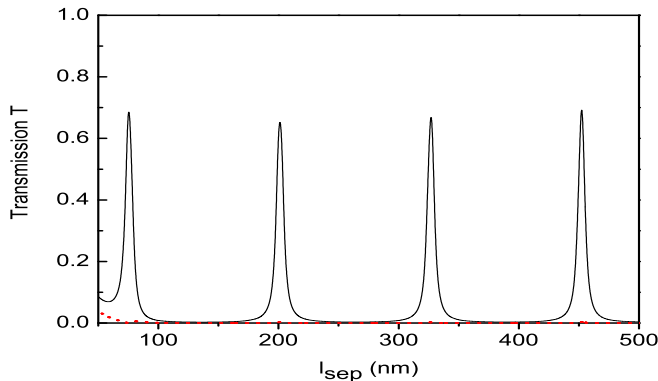


FIG. 10: Transmission through two InGaAs segments grown along the $[110]$ direction with $\alpha = \beta = \alpha_0$, versus the length ℓ_{sep} of the Rashba SOI-free region that separates them, for fixed $\ell_1 = \ell_2 = 95$ nm and energy $E = E_1 + 0.13$ meV. The solid curve shows the total transmission, and the dotted one the T^{+-} transmission.

Finally, we consider a WG grown along the $[110]$ direction that was treated theoretically in Sec. II B. The Dresselhaus term acquires the simple form $-2\beta\sigma_z k_x$ and, as was shown in Sec. III, this affects the dispersion relation significantly. We show numerical results for the transmission through two InGaAs segments separated by a Rashba SOI-free region in Fig. 10 when only one subband is occupied. The solid curve shows the total transmission and the dotted one, barely visible, the T^{\pm} transmission. As seen, the peak values are noticeably lower than in the previous case and the number of peaks is increased due to the different dispersion relation $E(k_y)$.

IV. CONCLUDING REMARKS

We presented results for the electron transmission T through WGs in which both terms of the SOI are present and the mixing of the first two subbands is taken into account. In general, the influence of subband mixing is to shift the (longitudinal) resonances and suppress the spin-down to spin-up transmission. Two growth directions were considered [010] and [110], with more attention given to the former. Further, changing the sign of the RSOI strength has a very strong filtering effect on the spin-down contribution while leaving the total transmission intact.

For two segments separated by a SOI-free region, of length ℓ_{sep} , T shows resonances, as a function of ℓ_{sep} , that are most pronounced for $\alpha = \beta$. When both subbands are occupied, the total transmission varies little and remains close to unity, so that the filtering effect is contained only in T^{+-} . Similar to the case when one subband is occupied, changing the sign of the Rashba strength reduces the spin-up to spin-down transmission, cf. Fig. 9. In addition, we took into account possible band offsets between these segments and the SOI-free region that separates them. As shown in Fig. 8, this reduces the amplitude of the transmission but does not affect its qualitative dependence on ℓ_{sep} , notice in particular the highly binary structure of the transmission in Fig. 8(b) and consequently that of the conductance (not shown) at least for very low temperatures as reflected by Eq. (23).

The transmission T and conductance G oscillate as a function of α , β , or α/β if α and β are sufficiently strong. In such a case a nearly square-wave form is shown in Fig. 6(c) for T and in Fig. 6(d) for G at temperature $T_0 = 0.2$ K. Both results are in line with those [15] for $\beta = 0$. For higher temperatures the qualitative behaviour of G remains the same but its maxima are a bit rounded off. Together with the control of α by a bias [4] and the independent one of β reported very recently [16], the results indicate that a realistic spin transistor is possible if the SOI-free regions are relatively narrow.

Acknowledgments

Our work was supported by the Canadian NSERC Grant No. OGP0121756.

- [1] Y. A. Bychkov and E. I. Rashba, *J. Phys. C* **17**, 6039 (1984).
- [2] R. Winkler, *Spin-orbit coupling effects in two-dimensional electron and hole systems*, Springer Tracts in Modern Phys. Vol. **191** (Springer, New York, 2003).
- [3] G. Dresselhaus, *Phys. Rev.* **100**, 580 (1955).
- [4] J. Nitta, T. Akazaki, H. Takayanagai, and T. Enoki, *Phys. Rev. Lett.* **78**, 1335 (1997); C-M Hu, J. Nitta, T. Akazaki, H. Takayanagi, J. Osaka, P. Pfeffer and W. Zawadzki, *Phys. Rev. B* **60**, 7736 (1999).
- [5] G. Engels, J. Lange, T. Schäpers and H. Lüth *Phys. Rev. B* **55** R1958 (1997).
- [6] D. Grundler, *Phys. Rev. Lett.* **84**, 6074 (2000).
- [7] E. L. Ivchenko, A. Y. Kaminski, and U. Rössler, *Phys. Rev. B* **54**, 5852 (1996).
- [8] O. Krebs, D. Rondi, J. L. Gentner, L. Goldstein, and P. Voisin, *Phys. Rev. Lett.* **80**, 5770 (1998).
- [9] S. D. Ganichev, V. V. Bel'kov, L. E. Golub, E. L. Ivchenko, P. Schneider, S. Giglberger, J. Eroms, J. De Boeck, G. Borghs, W. Wegscheider, D. Weiss, and W. Prettl, *Phys. Rev. Lett.* **92**, 256601 (2004); V. I. Perel, S. A. Tarasenko, I. N. Yassievich, S. D. Ganichev, V. V. Belkov, and W. Prettl, *Phys. Rev. B* **67**, 201304(R) (2003).
- [10] S. Datta and B. Das, *Appl. Phys. Lett.* **56**, 665 (1990).
- [11] J. Schliemann, J. C. Egues, and D. Loss, *Phys. Rev. Lett.* **90**, 146801 (2003).
- [12] S. Bandyopadhyay and M. Cahay, *Appl. Phys. Lett.* **85**, 1814 (2004).
- [13] I. Žutić, J. Fabian, and S. Das Sarma, *Rev. Mod. Phys.* **76**, 323 (2004).
- [14] X. F. Wang, P. Vasilopoulos, and F. M. Peeters, *Phys. Rev. B* **65**, 165217 (2002).
- [15] X. F. Wang and P. Vasilopoulos, *Appl. Phys. Lett.* **83**, 940 (2003).
- [16] J. D. Koralek, C. Weber, J. Orenstein, A. Bernevig, S. Zhang, S. Mack, and D. Awschalom, *Nature* **458**, 610 (2009).
- [17] N. S. Averkiev and L. E. Golub, *Phys. Rev. B* **60**, 15582 (1999).
- [18] X. F. Wang and P. Vasilopoulos, *Phys. Rev. B* **68**, 035305 (2003).

- [19] X. Cartoixà, L.-W. Wang, D. Z.-Y. Ting, Y.-C. Chang, Phys. Rev. B **73**, 205341 (2006); B. A. Bernevig, J. Orenstein, and S.-C. Zhang, Phys. Rev. Lett. **97**, 236601 (2006); M.-H. Liu, K.-W. Chen, S.-H. Chen, and C.-R. Chang, Phys. Rev. B **74**, 235322 (2006).
- [20] M. Wang, K. Chang, and K. S. Chan, Appl. Phys. Lett. **94**, 052108 (2009).
- [21] L. W. Molenkamp, G. Schmidt, and G. E. W. Bauer, Phys. Rev. B **64**, 121202(R) (2001).
- [22] H. Xu, Phys. Rev. B **47**, 9537 (1993).
- [23] For $N = 20$ the total length of the structure is $L_{tot} = 2\mu m$ and comparable to the phase relaxation length ℓ_ϕ which is about $0.7\mu m$, see Choi *et al.* Phys. Rev. B **36**, 7751 (1987). For larger N the implicit assumption $L_{tot} \leq \ell_\phi$ will not hold but one could reduce the unit length to satisfy this condition.
- [24] L. Lu, J. Wang, Y. Wang, W. Ge, G. Yang, and Z. Wang, J. Appl. Phys. **83**, 2093 (1998).
- [25] J. C. Fan and Y. F. Chen, J. Appl. Phys. **80**, 6761 (1996).